Available online at www.sciencedirect.com

ScienceDirect

Nuclear Physics A 1005 (2021) 121939

NUCLEAR PHYSICS A

www.elsevier.com/locate/nuclphysa

XXVIIIth International Conference on Ultrarelativistic Nucleus-Nucleus Collisions (Quark Matter 2019)

Latest results on the production of hadronic resonances in ALICE at the LHC

Arvind Khuntia (For the ALICE Collaboration)

The H. Niewodniczanski Institute of Nuclear Physics, Polish Academy of Sciences, PL-31342 Krakow, Poland
email:arvind.khuntia@cern.ch

Abstract

Measurement of short-lived hadronic resonances are used to study different aspects of particle production and collision dynamics in pp, p–A and relativistic heavy-ion collisions. The yields of resonances are sensitive to the competing processes of hadron rescattering and regeneration, thus making these particles unique probes of the properties of the late hadronic phase. Measurements of resonances with different masses and quantum numbers also provide insight into strangeness production and processes that determine the shapes of particle momentum spectra at intermediate transverse momenta, as well as the species dependence of hadron suppression at high momentum. We present the comprehensive set of results in the ALICE experiment with unprecedented precision for $\rho(770)^0$, $K^*(892)$, $\phi(1020)$, $\Sigma(1385)^{\pm}$, $\Lambda(1520)$, and $\Xi(1530)^0$ production in pp, p–Pb, Xe–Xe and Pb–Pb collisions in the energy range $\sqrt{s_{NN}}$ = 2.76-13 TeV, including the latest measurements from LHC Run 2. The obtained results are used to study the system-size and collision-energy evolution of transverse momentum spectra, particle ratios and nuclear modification factors and to search for the onset of collectivity in small collision systems. We compare these results to lower energy measurements and model calculations where available.

Keywords: Identified hadron yields, particle ratios, nuclear modification factor, pp, p–Pb, Xe–Xe, Pb–Pb

1. Introduction

At the LHC, measurements of various observables in p–Pb and pp collisions with high charged-particle multiplicity have shown remarkable similarities to corresponding measurements in heavy-ion collisions. The observation of azimuthal correlations amongst particles and anisotropic flow (V_2) in small collision systems indicate presence of collective effects. However, the origins of such effects in smaller collision systems lack explanation leaving the question whether the underlying causes are the same as in large collision systems such as Xe–Xe and Pb–Pb. Recent results show an enhancement in the production of strange hadrons; the ratio of yield of strange hadrons to non-strange hadrons show an increase with increasing charged particle multiplicity in pp collisions and the values of ratios in high multiplicity collisions approach the observed ratios in p–Pb and peripheral Pb–Pb collisions at similar multiplicities [1]. The strength of this enhancement increases with increasing strange quark content of the hadron rather than mass or baryon number in small

https://doi.org/10.1016/j.nuclphysa.2020.121939
0375-9474/

systems. The ϕ meson with net strangeness zero, can help to understand strangeness production in smaller collision systems. Comparison of ϕ-meson production relative to other hadrons with different strangeness content as a function of charged particle multiplicity in various collision systems may reveal information about the effective strangeness of the ϕ meson. Furthermore, resonances with short lifetimes are sensitive to the rescattering and regeneration process during the evolution of the fireball from chemical to kinetic freeze-out. An observable such as the nuclear modification factors of the resonances can help to understand the in-medium parton energy loss in heavy-ion collisions, and hence has paramount importance in understanding the particle production mechanism in high energy collisons.

2. Analysis details

The ALICE detector is described in detail in ref. [2]. The sub-detectors which are relevant to this analysis are the Time Projection Chamber (TPC), the Time-of-Flight detector (TOF), the Inner Tracking System (ITS) ($|\eta| < 0.9$), and the V0A ($2.8 < \eta < 5.1$) and V0C ($-3.7 < \eta < -1.7$) detectors. The TPC and ITS are used for tracking and finding the primary vertex, whereas the TPC and TOF are used for particle identification. The V0 detectors are used for triggering and estimation of multiplicity at forward rapidities [3]. The measurements of resonance, strange and multi-strange hadron production are carried out at mid-rapidity ($|y| < 0.5$ in pp, Xe–Xe and Pb–Pb collisions and $0 < y_{\rm cm} < 0.5$ in p–Pb collisions) as a function of the charged particle multiplicity. Resonances are measured via an invariant mass analysis from the hadronic decay daughters: $\rho^0 \rightarrow \pi^+\pi^-$(B.R. $\sim$ 100%), $\rm K^{*0}\rightarrow K^+\pi^-$ (66.6 %), $\phi \rightarrow \rm K^+K^-$ (49.2 %), $\Lambda \rightarrow$ pπ^- (63.9%), $\Sigma^{*+}(\Sigma^{*-}) \rightarrow \Lambda\pi^+(\Lambda\pi^-)$ (87%) and $\Xi^{*0} \rightarrow \Xi^-\pi^+$(66.7%) [4]. In the invariant-mass method the combinatorial background has been estimated by using an event-mixing technique for resonances, however a like-charge background is also used in some analyses. For strange and multi-strange hadrons, a set of topological cuts is applied to eliminate the background which do not fit the expected decay topology. The raw yields are extracted from the signal distribution after the subtraction of the combinatorial background and are corrected for the detector acceptance, tracking efficiency and branching ratio.

3. Results and discussion

The production of $\rho(770)^0$, $\rm K^*(892)$, $\phi(1020)$, $\Sigma(1385)^{\pm}$, $\Lambda(1520)$, and $\Xi(1530)^0$ in different multiplicity classes in pp, p–Pb, Xe–Xe and Pb–Pb collisions in the energy range $\sqrt{s_{\rm NN}}$ = 2.76-13 TeV have been measured in a wide range of transverse momentum. The $p_{\rm T}$-integrated hadron yields (dN/dy) and mean $p_{\rm T}$ ($\langle p_{\rm T}\rangle$) are determined by integrating the $p_{\rm T}$ spectra in the measured range and by using a fit function (Lévy-Tsallis or Blast Wave) to extrapolate the yields in the unmeasured $p_{\rm T}$ region for each multiplicity event class. Figure 1 shows the comparison of $\langle p_{\rm T}\rangle$ of $\rm K^{*0}$, ϕ and p as a function of charged particle multiplicity ($\langle {\rm d}N_{\rm ch}/{\rm d}\eta\rangle$) in pp collisions at $\sqrt{s}$ = 7 and 13 TeV, p–Pb at $\sqrt{s}$ = 5.02 and Pb–Pb at $\sqrt{s}$ = 2.76 TeV [5]. A similar increase in $\langle p_{\rm T}\rangle$ with the charged particle multiplicity is observed for pp collisions at $\sqrt{s_{\rm NN}}$ = 7 and 13 TeV. A clear mass ordering of $\langle p_{\rm T}\rangle$ is observed in central Pb–Pb collisions, where $\rm K^{*0}$, ϕ and p with

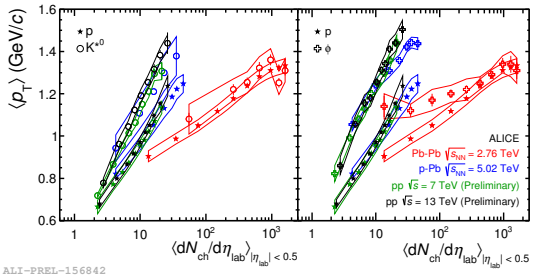

Fig. 1. (Color online) Mean transverse momentum ($\langle p_{\rm T}\rangle$) of $\rm K^{*0}$, ϕ and p in pp at $\sqrt{s}$ = 7 and 13 TeV, p–Pb at $\sqrt{s_{\rm NN}}$ = 5.02 TeV and Pb–Pb at $\sqrt{s_{\rm NN}}$ = 2.76 TeV collisions as functions of charged particle multiplicity. The bars and lines represent the statistical and the systematic errors, respectively.

similar masses have similar $\langle p_{\rm T}\rangle$ values, which is expected from the hydrodynamic expansion of the system [6]. However, the mass ordering of $\langle p_{\rm T}\rangle$ breaks down for the peripheral Pb–Pb and smaller collision systems. The normalized integrated yields of $\rm K^{*0}$ and ϕ to $\langle {\rm d}N_{\rm ch}/{\rm d}\eta\rangle$ in pp collisions at $\sqrt{s_{\rm NN}}$ = 7 and 13 TeV, and

p–Pb collisions at $\sqrt{s_{\rm NN}}$ = 5.02 and 8.16 TeV as a function of charged particle multiplicity are shown in Fig. 2. For both K^{*0} and ϕ, it is observed that the yields normalised to $\langle dN_{\rm ch}/d\eta\rangle$ have similar values at same charged particle multiplicity and are independent of collision energy in small collision systems. The ratio of

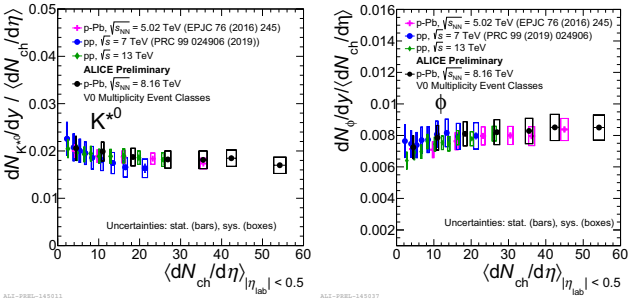

Fig. 2. (Color online) Integrated yields of K^{*0} (left panel) and ϕ (right panel) normalized to $\langle dN_{\rm ch}/d\eta\rangle$ in pp collisions (at $\sqrt{s}$ = 7 and 13 TeV) and p–Pb collisions (at $\sqrt{s_{\rm NN}}$ = 5.02 and 8.16 TeV) for different multiplicity classes. The bars and the boxes represent the statistical and systematic errors, respectively.

resonance yields to the yields of long-lived hadrons as a function of charged particle multiplicity for ρ^0/π, K^{*0}/K, $\Sigma^{*\pm}/\Lambda$, Λ^*/Λ, Ξ^{*0}/Ξ and ϕ/K in pp, p–Pb, Xe–Xe, and Pb–Pb collisions are shown in Fig. 3. The right panel shows the ratio of K^{*0}/K and ϕ/K as a function of charged particle multiplicity without log-scale for the better visibility and the right panel shows the particle ratios along with MC model comparisons. Significant suppression is observed for ρ^0/π, K^{*0}/K, and Λ^*/Λ with charged particle multiplicity in central Pb–Pb collisions. This is qualitatively explained by the EPOS generator with UrQMD, which attributes the suppression to the decay daughters in the hadronic phase of the collision [7, 8]. For pp collisions, the decreasing trend of K^{*0}/K with charged particle multiplicity hints at the possible presence of a hadronic phase with non-zero lifetime in small collision systems [9].

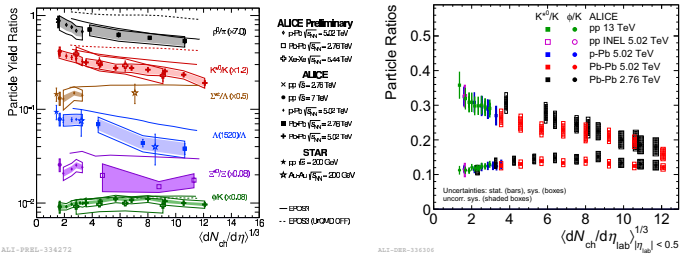

Fig. 3. (Color online) Resonance yield ratio to long-lived hadrons for pp, p–Pb, Xe–Xe, and Pb–Pb collisions, with comparisons to EPOS3 predictions and STAR data as a function of charged particle multiplicity ($\langle dN_{\rm ch}/d\eta\rangle$). (Left panel) The bars and the lines represent the statistical and systematic errors, respectively. (Right panel) The bars and the boxes represent the statistical and systematic errors, respectively.

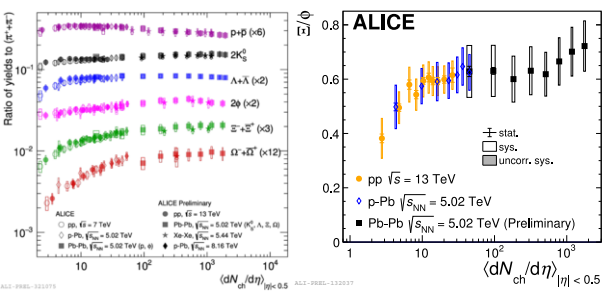

Fig. 4. (Color online) Left panel: Ratios of the integrated yields, $(p+\bar{p})/(\pi^+ + \pi^-)$, $2K^0_S/(\pi^+ + \pi^-)$, $(\Lambda + \bar{\Lambda})/(\pi^+ + \pi^-)$, $2\phi/(\pi^+ + \pi^-)$, $(\Xi^- + \bar{\Xi}^+)/(\pi^+ + \pi^-)$, $(\Omega + \bar{\Omega})/(\pi^+ + \pi^-)$, measured as a function of the charged particle density in pp (at $\sqrt{s}$ = 7 and 13 TeV), p–Pb (at $\sqrt{s_{\rm NN}}$ = 5.02 and 8.16 TeV), Xe–Xe (at $\sqrt{s_{\rm NN}}$ =5.44) and Pb–Pb (at $\sqrt{s_{\rm NN}}$ = 5.02 TeV) collisions. Right panel: Ratios of the integrated yields, Ξ/ϕ in pp collisions at $\sqrt{s}$ = 13 TeV, p–Pb and Pb–Pb collisions at $\sqrt{s_{\rm NN}}$ = 5.02 TeV. The bars and the boxes represent the statistical and systematic error, respectively.

The ratios of hadron yields to pions as a function of $\langle dN_{\rm ch}/d\eta\rangle$ in pp at $\sqrt{s}$ = 7 and 13 TeV, p–Pb at $\sqrt{s_{\rm NN}}$ = 5.02 and 8.16 TeV, Xe–Xe at $\sqrt{s_{\rm NN}}$ =5.44 TeV, and Pb-Pb at $\sqrt{s_{\rm NN}}$ = 5.02 TeV are shown in Fig. 4 [10, 11] (Left panel). We observe a smooth evolution of particle ratios with multiplicity in pp, p–Pb, Xe–Xe

and Pb–Pb collisions at $\sqrt{s_{\rm NN}}$ = 2.76 -13 TeV: for a given charged particle multiplicity strangeness production is independent of collision system and energy. The ϕ meson with net strangeness zero, is not subjected to the canonical suppression while the production of hadrons with open strangeness may be canonically suppressed. However, it is rather difficult to describe enhancement of ϕ meson production in a framework that involves canonical suppression [5]. In models that use core-corona [12] and rope-hadronization pictures [13], the evolution of ϕ meson yields with charged particle multiplicity is similar to the behaviour for particles of open strangeness, making it possible for the measurement to provide explanations for enhancement in small systems. The ϕ meson production relative to pions increases with charged particle multiplicity as shown in Fig. 4 and also a mild enhancement for ϕ/K ratios for small collision systems. For the Ξ/ϕ ratio shown in Fig 4 (Right panel) we see a flat or mild increasing trend for a wide range of multiplicity classes. These results suggests that the ϕ-meson behaves as a particle with an effective strangeness of 1-2. Figure 5 shows the nuclear modification factor as a function of $p_{\rm T}$ for $\rm K^{*0}$ and ϕ mesons in $0-5\%$ centrality in Pb–Pb collisions at $\sqrt{s_{\rm NN}}$ = 2.76 TeV [14, 15]. Similar suppression is observed for different light flavour hadrons above $p_{\rm T} \simeq 10$ GeV/c. Mass ordering is observed for $R_{\rm AA}$ at intermediate $p_{\rm T}$ among mesons, which may be attributed to the effect of radial flow.

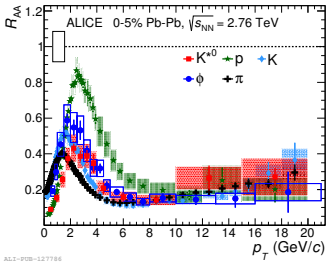

Fig. 5. (Color online) The nuclear modification factor $R_{\rm AA}$, as a function of $p_{\rm T}$ for $\rm K^{*0}$ and ϕ mesons in $0-5\%$ centrality in Pb–Pb collisions at $\sqrt{s_{\rm NN}}$ = 2.76 TeV.

4. Summary

ALICE has extensive results on production of resonances with lifetimes 1.3-46.4 fm/c in different collision systems. The particle yields have similar values for a given charged particle multiplicity: hadrochemistry is driven by event multiplicity rather than by colliding system and collision energy. Mass ordering of $\langle p_{\rm T} \rangle$ is observed in central Pb–Pb collisions, which is expected from the hydrodynamic expansion of the system. However, this mass ordering breaks down for the peripheral Pb–Pb and smaller collision systems. Suppression in particle yield is observed for short-lived resonances relative to more stable particles, ρ^0, $\rm K^{*0}$, and Λ^* (τ < 13 fm/c) in most central A–A collisions, whereas no suppression for the ϕ (τ = 46.4 fm/c) meson. The suppression in A–A collisions is attributed to the dominance of rescattering in the hadronic phase. A hint of suppression for $\rm K^{*0}$/K in high multiplicity pp and p–Pb collisions suggests the presence of rescattering effects in high multiplicity pp and p–Pb collisions, which can be compared to Pb–Pb collisions with similar charged particle multiplicity. The ϕ/K ratio shows mild increasing trend with multiplicity in pp collisions whereas Ξ/ϕ shows an increasing trend over a wide range of multiplicity. These results together suggest that ϕ meson behaves as a particle with an effective strangeness between 1 and 2. Suppression of $R_{\rm AA}$ for different light flavour hadrons including resonances above $p_{\rm T} \simeq 10$ GeV/c is similar, which indicates that parton energy loss at high $p_{\rm T}$ is species independent.

[1] J. Adam *et al.* (ALICE Collaboration) Nature Physics **13**, (2017) 535–9.
[2] B. B. Abelev *et al.* [ALICE Collaboration], Int. J. Mod. Phys. A **29**, 1430044 (2014).
[3] B. Abelev *et al.* (ALICE Collaboration) Phys. Rev. C **88**, (2013) 044909.
[4] M. Tanabashi *et al.* [Particle Data Group], Phys. Rev. D **98**, 030001 (2018).
[5] S. Acharya *et al.* [ALICE Collaboration], Phys. Rev. C **99**, 024906 (2019).
[6] C. Shen, U. Heinz, P. Huovinen, and H. Song, Phys. Rev. C **84**, (2011) 044903.
[7] A. G. Knospe, C. Markert, K. Werner, J. Steinheimer and M. Bleicher, Phys. Rev. C **93**, 014911 (2016).
[8] S. Acharya *et al.* [ALICE Collaboration], arXiv:1910.14419 [nucl-ex].
[9] S. Acharya *et al.* [ALICE Collaboration], arXiv:1910.14397 [nucl-ex].
[10] J. Adam *et al.* [ALICE Collaboration], Phys. Lett. B **758**, 389 (2016).
[11] B. B. Abelev *et al.* [ALICE Collaboration], Phys. Lett. B **728**, 25 (2014).
[12] K. Werner, B. Guiot, I. Karpenko and T. Pierog, Phys. Rev. C **89**, 064903 (2014).

[13] T. S. Biro, H. B. Nielsen and J. Knoll, Nucl. Phys. B **245**, 449 (1984).
[14] J. Adam *et al.* [ALICE Collaboration], Phys. Rev. C **93**, 034913 (2016).
[15] J. Adam *et al.* [ALICE Collaboration], Phys. Rev. C **95**, 064606 (2017).